

AD-785 610

VAPORIZATION WAVES IN IMPULSIVELY
HEATED MATERIALS

Henry S. Burden

Ballistic Research Laboratories
Aberdeen Proving Ground, Maryland

1972

DISTRIBUTED BY:

NTIS

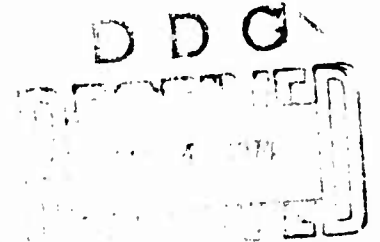
National Technical Information Service
U. S. DEPARTMENT OF COMMERCE
5285 Port Royal Road, Springfield Va. 22151

AD 785610

VAPORIZATION WAVES IN IMPULSIVELY
HEATED MATERIALS

HENRY S. BURDEN, MR.

U. S. ARMY BALLISTIC RESEARCH LABORATORIES
ABERDEEN PROVING GROUND, MARYLAND



1. INTRODUCTION

Computer hydrocodes are essential in determining the magnitude, transmission, and effects of stresses produced when energy is impulsively deposited in a material. As do any solutions of the hydrodynamic equations, these numerical approaches depend upon the form of an auxiliary equation of state for their success. Most hydrocodes give satisfactory treatment in the solid and liquid phases but in codes (1) such as PUFF and RIP the equations of state ignore or improperly treat the liquid-vapor phase change region in which the major expansion of subcritically heated materials takes place. In this paper, a model for this expansion is described which was successful in resolving an anomaly in exploding wire response (2) but is of a type that could not be duplicated by hydrocodes using these equations of state. With refinement, this vaporization wave model can be applied to determining thermodynamic data that will aid in revising the equations of state for materials of interest. These improvements will have relevance to the response of metals impulsively converted to vapor by absorption of radiation, whether it be from laser, electron beam, nuclear, or other sources.

2. IMPULSIVE HEATING

If a substance is so rapidly heated that the normally associated expansion is prevented by the material's own inertia, pressure will be built up in its interior and maintained at any point until an expansion wave originating at a free surface has had time to penetrate to that point. A representative P- ρ diagram (3) (Figure 1)

BURDEN

may be used to describe the expansion following such heating. To place it in our realm of interest, we will choose a process which causes the material to enter the liquid vapor coexistence state. Such a process may be imagined as follows: the point describing the state of a material will, if the material is heated instantaneously, jump from its room temperature, uncompressed position vertically until it reaches a new position representing an unchanged density and lying on a contour marked with the value of heat energy added, e.g., $E=2000$ cal/g. This would correspond on the diagram of Figure 1 to a pressure on the order of 400 kbar ($1 \text{ bar} = 10^6 \text{ dyne/cm}^2 \cong 1 \text{ atm}$). Then, if the expansion takes place over a period less than a few microseconds, negligible heat will be lost from the material by radiation or conduction and we may follow the energy contour (adiabat) as the material expands to lower values of density. However, material at no point except on a free surface may expand unless adjacent material is moving away to make room for it. Thus, an expansion setting the material in motion starts at a free surface and moves inward as a wave; the velocity of such a wave at any point may be shown (2) equal to the square root of the local value of the slope $dP/d\rho$ along the adiabat there. (NOTE: Slopes measured directly from Figure 1 are $d(\ln P)/d(\ln \rho) = (dP/d\rho) (\rho/P)$.) If the material is heated uniformly, one adiabat will characterize the entire volume of material; if not, the heat energy deposited at each point will determine the adiabat descriptive of that point. For simplicity, assume in our imaginary example that the material is semi-infinite with one free surface and that heating is uniform throughout at 2000 cal/g. At some chosen interior point, a high pressure will exist until sufficient time has elapsed for an expansion front to reach it traveling from the free surface inward at a speed appropriate to the adiabat (see Figure 1). The pressure and density at this point will then fall, following the steep course of the adiabat until the liquidus line bounding the mixed liquid vapor region is reached. Here, there is a discontinuity in the slope of the adiabat. The expansion wave velocity is decreased by an order of magnitude, reflecting the highly compressible nature of the foam formed as liquid turns to vapor.

Figure 2 shows this front and the succeeding fan and Figure 3 illustrates the effect of the delay between passage of the liquid expansion and arrival of the mixed phase expansion in maintaining the pressure or density. The large change in density accompanying the second fan results in a large decrease in the electrical conductivity of the material. This is responsible in exploding wires for current "dwells" (4) during which field strengths from 5-10 kV produce insignificant current flow.

BURDEN

3. EXPERIMENT

In the experiments to be described, the semi-infinite sample is approximated by surrounding the edges and back surface of a thin, wide sample ribbon with a dense support material. The front surface is irradiated by an intense electron beam and, being unsupported, is free to expand. To detect the inward running expansion wave, a nominally constant current is directed lengthwise through the sample; as the advancing wave consumes the unexpanded, conducting material, the sample resistance rises, thus developing a proportional voltage increase. Copper and aluminum samples, as used in our experiments, are shown in Figure 4. All samples were 0.51 cm wide; thicknesses ranged from 0.005 to 0.015 cm. Figure 5 shows a cross-section of the construction of these assemblies. The substrate is a composite consisting of a 0.32 cm thick copper base (1 cm wide by 6 cm long) to which a 0.005 cm layer of fused silica was attached with the thinnest practicable (~ 0.0025 cm) layer of epoxy cement. The thickness of the base was limited by the penetration time of the beam-guiding magnetic field to avoid distortion of that field near the sample. The sample, and also, on either side of it, fused silica retaining walls, were attached to the electrically insulating, fused silica portion of the substrate. On the back side of the base, a thin copper ground strap and lead flyer plates, $\sim 0.3 \times 0.7 \times 1.6$ cm, were attached. The ground strap connected the signal cable shields to a reference connection at the center of the sample--which was also, approximately, at the center of symmetry of the beam. The flyer plates were designed to break loose and to carry away momentum transmitted by compression waves traveling through the substrate and the ground strap. This prevented voltage inducing motion of the ground strap in the beam guiding field and diminished reflections of stress waves from the back surface of the base.

The exciter current of ~ 33 A was produced by a 1 ms RC discharge and during the ~ 10 μ s experiment time was constant within about 15 percent. Its connection to the ends of the sample is diagrammed in Figure 6. The sample's grounded center tap was necessary to satisfy a requirement for symmetry imposed by the nature of the electron beam; it effectively created two samples. Leads to carry the voltage signals produced by the vaporizing ribbon were attached near each end, distinctly separated from the current connections to avoid any contact voltages. These leads' coaxial shields, though not shown, were connected via the ground straps noted earlier to the center tap. A low pass (<10 MHz) filter in each lead removed the large inductive pulses accompanying turn-on and turn-off of the beam current. One of the dual beam oscilloscopes, triggered internally, recorded signals from both sample halves using a high sweep rate; the other, initiated

BURDEN

by a trigger from the pulser, recorded both signals at a slow sweep rate. This arrangement reflects difficulty experienced in achieving proper triggering.

The pulser used was the Physics International SNARK (5). Its beam guiding solenoid was pulsed prior to discharge of the two parallel-plate, water insulated lines that power the beam. As the beam passed through the solenoid's converging, longitudinal field, it was first constricted and intensified and then expanded and weakened (as indicated in Figure 6). Thus, by a change of position, the sample could be subjected to a variety of intensities (or fluences) (6); the range chosen, expressed in terms of fluence absorbed in the sample, was from 44 to 111 cal/cm². The beam energies varied from 689 to 843 keV. As accompanying effects, the mean angle of incidence of the electrons varied between 30° and 40° and the beam diameter, between 4.4 and 5.6 cm.

Figure 7 shows rear and front views of the sample holder. Below the graphite shield ring attached in the front (right hand) view, the diametrically oriented sample with its center tap screw in place may be seen. On either side of the sample, 1 cm circles--the tops of cylindrical, graphite calorimeters--are exposed. The back (left hand) view of the holder shows two 0.6 cm thick stainless steel plates between which the sample substrate was clamped. Shallow, circular recesses machined in each plate accommodated the ends of an array of thermoluminescent detectors (TLD), one of which is shown (below the rear-view) in its acrylic plastic positioner. A collimating aperture in the center of each recess was drilled through to the front surface of the plate. A 0.0025 cm thick tantalum foil covered the entire irradiated front surface, except for the areas of the calorimeters and of the sample assembly, and converted the electron flux to x-rays. After passing through a 0.15 thick graphite filter, which stopped all electrons, the x-rays entered the collimating apertures and then excited the TLD's. Later "reading" of the TLD's provided a measure of beam uniformity which, from shot to shot varied between + 5% and + 20% (6).

Figure 8 shows representative sample-response curves. The upper pair of records represents slow and fast sweep traces for a nominally low energy exposure. The noise level exhibited is the lowest experienced. The slow-sweep oscilloscope was pretriggered and the first burst of noise observed coincided with the triggering of the pulse line charging unit; the second burst coincided with the beam turn-on. The traces marked "Sample 1" and "Sample 2" represent responses of the two halves of the center tapped sample. The lower pair of records was representative of the worst of those considered

BURDEN

readable. The difficulty in determining amplitudes or initiation times accurately is evident. The reading approach used was to average the peak excursions, either numerically or visually, depending on their severity. The auxiliary sensing current records were correlated in time so that a resistance history could be deduced from the voltage signals.

4. INTERPRETATION OF DATA

An expression relating oscillographically measured quantities, on the left side, to physical quantities on the right

$$R^{-2} dR/dt = (w/l) [c(e)/\rho(e)] \quad (1)$$

may be easily derived using the two relations

$$R = \rho l/w(x_f - x)$$

and

$$c = dx/dt$$

where R = measured resistance (ohms), t = measured time (s), c = velocity of expansion front (cm/s), ρ = resistivity (ohm-cm), e = specific energy (J/g), w = width of sample (cm), x_f = thickness of sample (cm), x = depth below irradiated surface (cm), and l = length of sample (cm). Inductive voltages developed across the sample have been considered negligible in this treatment in part because the sensing current is not changing rapidly and in part because the rate of change of inductance (7) related to the changing thickness of the conducting material has been rendered small by the use of relatively broad ribbons. The latter voltage, in its worst case, is on the order of 2% of the measured resistive voltage. The sensing current distribution in the samples after heating is predicted by transient skin effect theory (8) to have effectively reestablished equilibrium in about 75 ns for 0.0102 cm thick copper samples and 125 ns for the 0.0152 cm thick aluminum samples--the thickest of each type. These times are on the order of the 100 - 120 ns beam duration times and, at most, a small percentage of the 1-10 μ s running times of the vaporization waves.

It should be noted that the heating is not uniform with depth, thus pressure gradients exist which may allow internal expansions; the front surface expansion appears, however, to remain dominant in pressure relief.

BURDEN

A discrete discontinuity in conductivity at the vaporization front has been implied in the derivation, but it appears likely that there is a more diffuse region of change centered somewhere in the expansion fan and traveling at a velocity close to that of the expansion front. Further, the heating is not instantaneous, but takes a small fraction of the expansion's traverse time. Nor is the medium supporting the wave stationary: the deposition is such that the front surface of the sample, having expanded through the solid and liquid phases, may be moving with a velocity on the order of the vaporization wave velocity, and front and rear surfaces may be diverging with a velocity one tenth of that. We neglect this relative motion and assume that the expanding substrate maintains pressure at the sample's back surface.

Two approaches to interpretation of the data have been used and each makes use of data from exploding wire experiments. These data have been fitted to polynomials and express wave speed and resistivity as functions of specific energy. For copper

$$c = 4229. -6.534e + 0.02524e^2$$

and

$$\rho = 2.047 \times 10^{-5} [1 + 4.769 \times 10^{-4} (e - 1090.)].$$

For aluminum

$$c = 11,353. -6.370e + 0.000876e^2$$

and

$$\rho = 4.045 \times 10^{-5} [1 - 1.620 \times 10^{-4} (e - 3548.)].$$

For each experimental value of $R(t)$, a value of e may then be found. Corresponding values of c may be calculated and integrated over time to yield values of x .

Such data is plotted in Figures 9, 10, and 11 which also compare similar curves determined independently, by more conventional methods at the Physics International Co. (6) The agreement in results suggests the use of ribbon samples as deposition profile gages.

An alternate treatment of the data provided a determination of the velocity function $c = c(e)$, quasi-independently of the exploding wire experiment. It had to depend on the resistivity

BURDEN

function $\rho = \rho(e)$ determined by that experiment since this type of information could not be extracted from the present experiment. The specific energy came from among six normalized deposition profiles calculated using a condensed case history Monte Carlo electron transport code. Profiles were computed for the combinations of two mean angles of electron incidence and three beam voltages. The values plotted were obtained after three steps: interpolation between profiles to actual conditions of the test, application of a correction for the fused silica substrate, and representation of the result by a two-segment, polynomial fit. (The "dosimetry" curves of Figures 9-11 are plots of these normalized curves scaled by measured fluence.)

The experimental resistance data was converted to velocity by the use, again, of Equation 1. Now a resistivity corresponding to a trial value of energy was used to calculate c and $x (= \Sigma c \Delta t)$. This trial value was then compared with the polynomial value $e(x)$ and adjusted by an iterative loop until internal consistency was achieved.

Figures 12, 13, and 14 show these results and, for comparison, plots of the exploding wire wavespeed versus energy polynomials.

Fluence measurements were made using thermoluminescent detectors (TLD) (whose precision was $\pm 3\%$) calibrated against the average of a large number of carbon calorimeters (whose accuracy was $\pm 10\%$). Normalized deposition profiles were calculated with a precision estimated at $\pm 10\%$. Specific energies were thus quoted with an accuracy estimated at $\pm 15\%$ by the Physics International Co. Measurements employing a stacked carbon foil depth-dose gage, when scaled to the areal density of copper, generally agreed with the calculated profile (6).

The nominal precision of the exploding wire data is about $\pm 8\%$. The portion of the data used in determining the resistivity function occupied only a few percent of full scale; thus, it is not surprising to find variations from shot to shot of $\pm 30\%$. This points to a need for improving this data.

Neither the triggering nor the electrical noise isolation was good in the data obtained. Consequently, in the pre-triggered, slow sweep shots it was difficult to see the experiment initiation time to within $0.1 \mu\text{s}$; there was even greater uncertainty in the internally triggered, fast sweep shots since it is not clear which event actually triggered the sweep. Finally, noise almost totally obscured the first $0.3 - 1 \mu\text{s}$ after initiation and made the accuracy of reading of the early amplitudes 10 to 30% at best.

BURDEN

5. ASSESSMENT

Those results presented in Figures 9-14 are selected from 15 copper and 2 aluminum exposures; the copper results are generally representative of the extremes in deposited energies. This experiment, depending as it does upon externally generated data for its interpretation, serves to relate the sources of this data if the physical process is properly described. It appears (assuming that the external data is correct) that the description is good at energies near the vaporization threshold for copper ($\sim 1400\text{J/g}$) and not so good at energies twice this value. This trend, with exceptions, was observed throughout the data. The vaporization thresholds for the low energy copper and the aluminum samples (Figure 12 and 14) are remarkably close to those found in static, atmospheric-pressure experiments (9).

In relating exploding wire and electron beam results, notice should be taken of their relative heating times. The nominal heating time for the electron beam ($\sim 100\text{ ns}$) is 1/5 to 1/10 that for the exploding wire, and the corresponding trajectories through the nonlinear state diagram are different. Thus, it is probable that a different value of the terminal velocity of the medium results from the expansion through the solid and liquid phases.

An interesting correlation occurred in three cases between pre-exposure observations of improper bonding of sample or side retaining walls and failures of the half of the sample in which it occurred. This is interpreted as evidence that the support material was performing the intended function and that, normally, expansion from the free surface did account for sample response.

A large potential source of error in results lies in the resistivity function, whose error bounds are large. In fact, a 20% increase in resistivity brings experimental deposition profiles into notably better alignment with the dosimetric values for copper. However, except for the data of Knoepfel and Luppi (10) which is on the order of 10% higher, no justification exists for revising it. More accurate determinations of this function are called for.

The integration of calculated velocities as reflected in the x-coordinates of Figures 9-11 provides an interesting and demanding self-check on the validity of the interpretation. Although considerable scatter is found between the calculated depths of penetration and the vaporization threshold depths of the transport code, in no case does the penetration of the wave exceed the thickness of the sample. This is despite the errors introduced into the higher,

BURDEN

early time velocities by electrical noise and may in part be attributed to the highly stable nature of the e versus x calculations which tends to correct for earlier velocity errors.

6. CONCLUSIONS

The program described has provided a means for experimental contact with the adiabats in the mixed-liquid-vapor regime of the equations of state for two metals. Because of the high temperatures and pressures necessary, these adiabats are not accessible by static processes.

The significant achievement of the series of tests is that a thermodynamically described phenomenon, which had served to explain the response of exploding wires, could be used to predict the unique response actually found in samples irradiated by a vaporizing electron beam. It is also significant that, when analyzed, this response could be inverted to describe to a reasonable, though not high, degree of accuracy the input conditions producing it.

The model used and the experimental techniques require refinement. Computer hydrocodes with realistic equations of state should provide a more precise model and an effort is being commenced in which one or more modifications to the equations of state available to the RIP hydrocode will be made. Options are (a) incorporation of the Goodwin equation of state (3), (b) revision of the presently incorrect tabular mixed-liquid-vapor sound speeds used in the RIP equation of state (1), and (c) modification of the GRAY (11) equation of state to describe the mixed-liquid-vapor region using a physically consistent approach developed by Kahl (12).

Also, further more accurate work in determining the resistivity function and in obtaining cleaner experimental signal traces is planned.

BURDEN

REFERENCES

1. R. H. Fisher and H. E. Read, "RIP, A One-Dimensional Material Response Code," SSS-R-72-1324, Sep 72 (Systems, Science, and Software, La Jolla, California 92037).
2. F. D. Bennett, G. D. Kahl, and E. H. Wedemeyer, "Resistance Changes Caused by Vaporization Waves in Exploding Wires," in Exploding Wires, Vol. 3, W. G. Chace & H. K. Moore, Ed., (New York, Plenum Press) 1964.
3. L. K. Goodwin, L. A. Johnson, and R. S. Wright, "An Equation of State for Metals," DASA-2286, Apr 69 (Aeronutronic Div. of Philco Ford Corp., Newport Beach, California 92660) NTIS Order No. AD858302L.
4. R. J. Reithel, J. H. Blackburn, G. E. Seay, and S. Skolnick, "The Current Pause in an Exploding Wire," in Exploding Wires (Vol. 1.) W. G. Chace and H. K. Moore, Ed., (New York, Plenum Press, Inc.) 1959.
5. S. Shope, P. Spence, and C. Stallings, "SNARK Electron Beam Development for Materials and Structures Irradiation," PIFR-301, June 1972 (Physics International Co., San Leandro, California 94577).
6. P. Spence, "Electron Beam Test Support for Mixed Phase Expansion Velocity Measurement," PITR-362, Sep 72 (Physics International Co., San Leandro, California 94577).
7. Page 5-28, American Institute of Physics Handbook, Dwight E. Gray, Coord. Ed., (New York, McGraw-Hill) 1957.
8. F. D. Bennett and J. W. Marvin, "Current Measurement and Transient Skin Effects in Exploding Wire Circuits," Rev. Sci. Inst. 33, 1218 (1962).
9. See Ref. 7, pages 4-42 and 4-130.
10. H. Knoepfel and R. Luppi, "The Electrical Conductivity of Metals at Very High Temperatures," in Exploding Wires, Vol 4, W. G. Chace and H. K. Moore, Ed., (New York, Plenum Press) 1968.
11. E. B. Royce, "Gray, A three-Phase Equation of State for Metals," UCRL-51121, September 1971.
12. G. D. Kahl, "Generalization of the Maxwell Criterion for Van Der Waals Equation," Phys Rev 155 (2), 78 (1967).

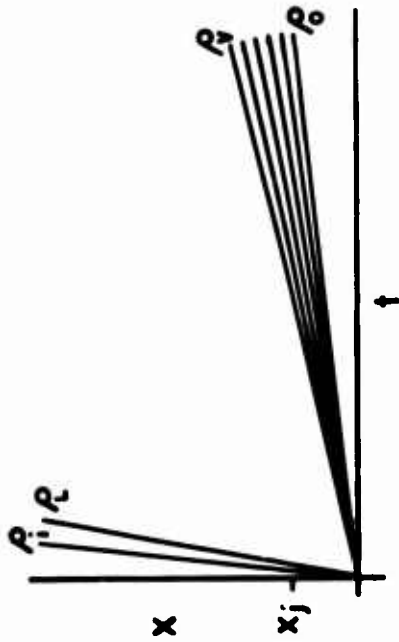


FIGURE 2. Expansion Fans on Depth (x) Versus Time (t) Plot Representative of Liquid (ρ_i to ρ_L) and Mixed-Liquid-Vapor (ρ_V to ρ_o) Expansions.

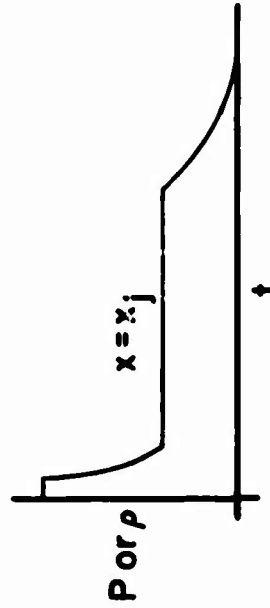


FIGURE 3. Qualitative Representation of Pressure (P) or Density (ρ) versus Time at Point x_j of Figure 2. (Vertical Scales Highly Nonlinear).

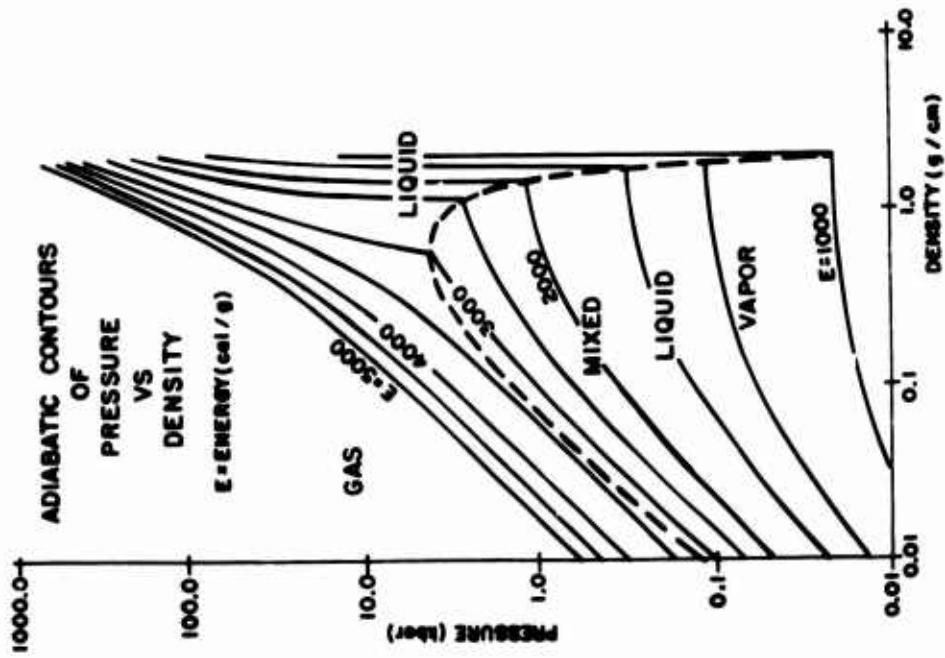


FIGURE 1. Pressure-Density (P - ρ) Diagram for Aluminum (3) Showing Constant-Energy (Adiabatic) Contours.



FIGURE 4. Copper and Aluminum Ribbon Samples Mounted on Copper Base Blocks.

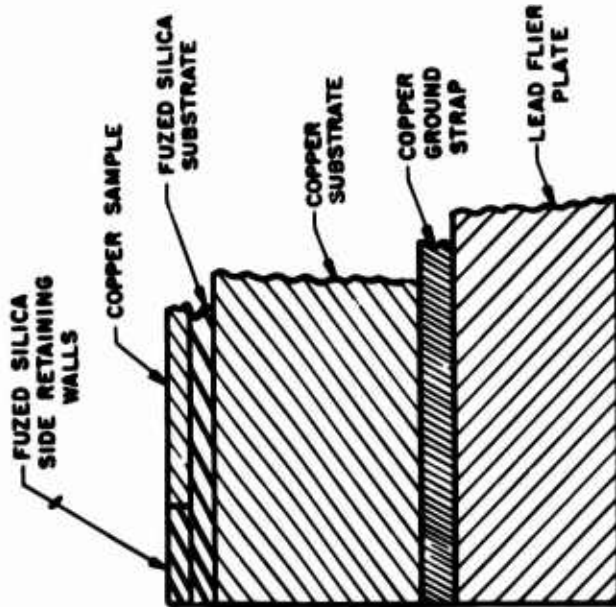


FIGURE 5. Diagram of Sample Holder Assembly. (Not to Scale.)

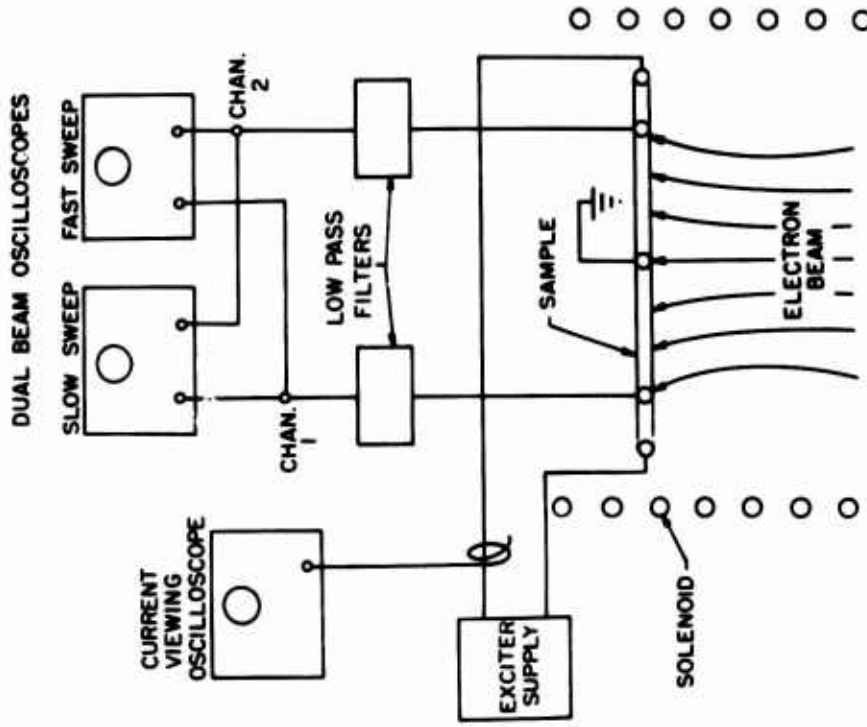


FIGURE 6. Basic Elements of Experimental Arrangement.



FIGURE 7. (Right) Sample Holder Completely Assembled. (Upper Left) Rear Face of Disassembled Holder Showing TLD Recesses. (Lower Left) Typical TLD Array.

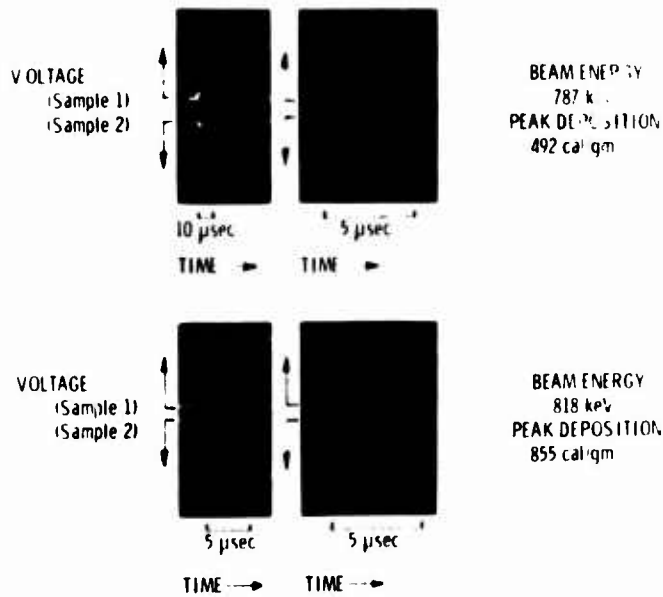


FIGURE 8. Oscillographic Data Trace Sets Showing Voltage Response of Two 0.0056 cm Thick, Center-Tapped Ribbons at Slow and Fast Sweeps.

BURDEN

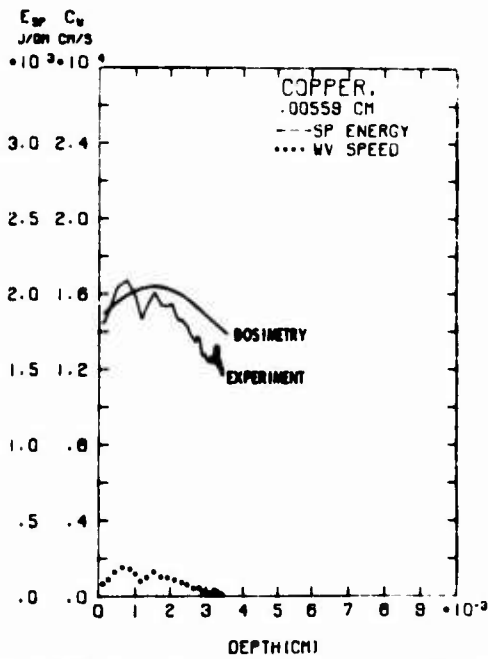


FIGURE 9. Specific Energy (E_{sp}) and Wave Speed (C_w) versus Depth in Copper at 48 cal/cm² Absorbed.

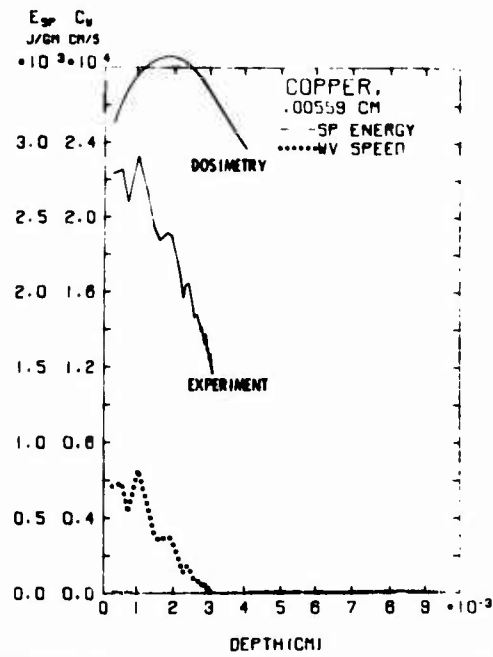


FIGURE 10. Specific Energy (E_{sp}) and Wave Speed (C_w) versus Depth in Copper at 90 cal/cm² Absorbed.

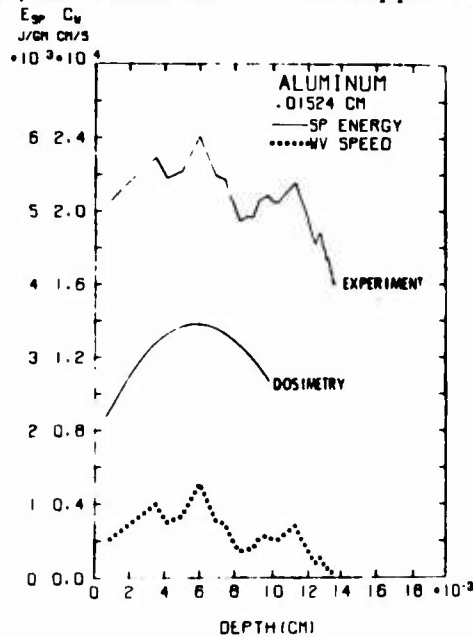


FIGURE 11. Specific Energy (E_{sp}) and Wave Speed (C_w) versus Depth in Aluminum at 91 cal/cm² Absorbed.

BURDEN

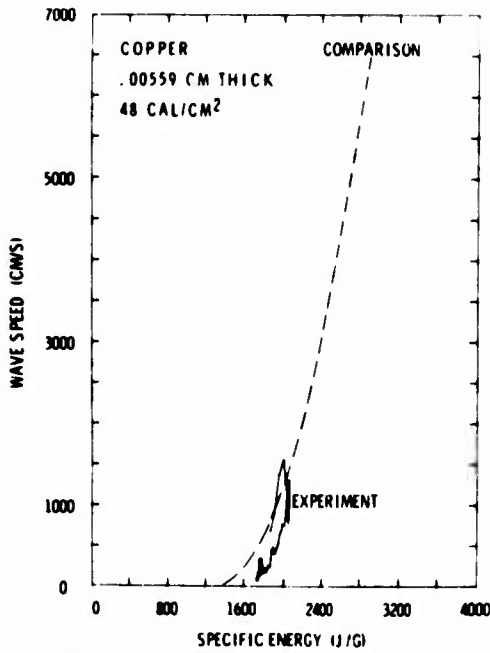


FIGURE 12. Measured Wave Speeds versus Specific Energy Compared with Exploding Wire Data Fit.

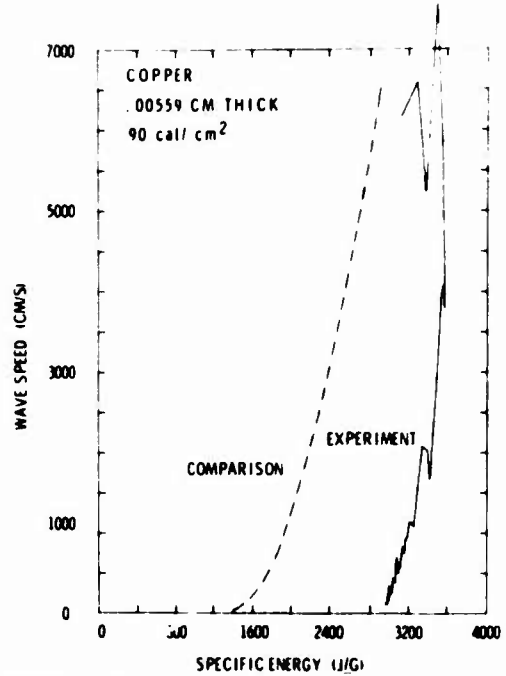


FIGURE 13. Measured Wave Speeds versus Specific Energy Compared with Exploding Wire Data Fit.

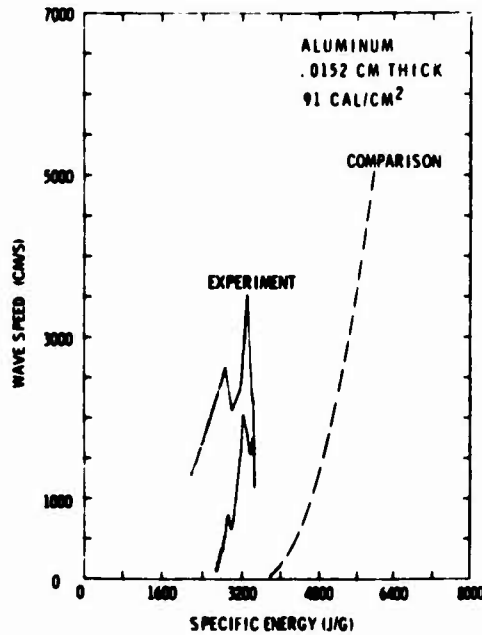


FIGURE 14. Measured Wave Speeds versus Specific Energy Compared with Exploding Wire Data Fit.